Journal Pre-proof

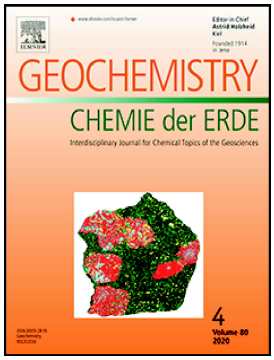

Coprecipitation of Ce with lead phosphates

Kacper Staszel, Julia Sordyl, Bartosz Puzio, Maciej Manecki

PII: S0009-2819(25)00007-8

DOI: https://doi.org/10.1016/j.chemer.2025.126252

Reference: CHEMER 126252

To appear in: *Geochemistry*

Received date: 29 July 2024

Revised date: 8 January 2025

Accepted date: 17 January 2025

Please cite this article as: K. Staszel, J. Sordyl, B. Puzio, et al., Coprecipitation of Ce with lead phosphates, *Geochemistry* (2025), https://doi.org/10.1016/j.chemer.2025.126252

This is a PDF file of an article that has undergone enhancements after acceptance, such as the addition of a cover page and metadata, and formatting for readability, but it is not yet the definitive version of record. This version will undergo additional copyediting, typesetting and review before it is published in its final form, but we are providing this version to give early visibility of the article. Please note that, during the production process, errors may be discovered which could affect the content, and all legal disclaimers that apply to the journal pertain.

© 2025 Published by Elsevier GmbH.

Journal Pre-proof

Coprecipitation of Ce with lead phosphates

Kacper Staszel [1*], Julia Sordyl [1,2], Bartosz Puzio [1], Maciej Manecki [1]

[1]AGH University of Kraków, Department of Mineralogy, Petrography and Geochemistry, al. Mickiewicza 30, 30-059 Kraków, Poland

[2]Uppsala University, Department of Earth Sciences, Villavägen 16, SE-752 36 Uppsala, Sweden

*corresponding author: kstaszel@agh.edu.pl (K. Staszel)

Abstract

Current development of sustainable technologies creates a demand for new sources of Rare Earth Elements (REE). Recent studies suggest that coprecipitation in the form of Pb-phosphates is one of the most effective methods in REE removal from aqueous solutions. This work focuses on the experimental study of the mechanisms of Ce coprecipitation with Pb phosphates, in particular with lead apatite - pyromorphite ($Pb_5(PO_4)_3Cl$). Coprecipitation experiments were conducted at ambient conditions, at pH range 1-11, by mixing solutions containing high concentrations of Pb and Ce (~66700 ppm and ~7600 ppm, respectively) with solutions containing stoichiometric concentrations of PO_4 and Cl. As a result of coprecipitation with Pb phosphates, the Ce concentration decreased significantly to less than 2 ppm. The main product of the coprecipitation was Ce-doped pyromorphite (Pym-Ce). Removal of Ce was most effective under alkaline conditions, while performance was slightly worse under acidic conditions, due in part to the slightly higher solubility of the precipitate. This was compared with a series of control experiments in the absence of either Pb, Cl, or Ce. Precipitation in the absence of Pb resulted in the formation of fibrous rhabdophane-Ce. In the absence of Cl, various phases were formed depending on pH conditions, such as 'phosphoschultenite' ($PbHPO_4$), Pb-hopeite ($PbPb_2(PO_4)_2 \cdot nH_2O$), mixed Pb and Ce hydrous phosphates, and hydroxylpyromorphite ($Pb_5(PO_4)_3OH$). In the absence of Ce, pure microcrystalline pyromorphite precipitated. Coprecipitation of Ce with Pb phosphates in the presence of Cl is advantageous due to the recovery of almost all Ce from solution in the form of a micro-crystalline Pym-Ce that is a very stable, insoluble phase easily separated from suspension. The precipitation of

Pym-Ce is homogenous over a wide range of pH, assuring consistency in the obtained phases regardless of starting conditions. Achieved high Ce removal levels may be crucial for the progress of the REE extraction industry, in terms of this method being applicable to other REE for their recovery from solutions, including apatite leachates.

Keywords: Rare earth elements, pyromorphite, Pb-apatite, apatite leaching, REE beneficiation

1. Introduction

Ongoing development and implementation of new green and sustainable technologies creates an ever increasing demand for Rare Earth Elements (REE). Their uneven distribution in Earth's crust resulting in lack of economically profitable primary sources, coupled with Chinese near monopolization of REE market, forces researchers in industrial and scientific fields to find new sources and develop new technologies. In past years, various methods for REE recovery have been intensively studied and developed, such as hydro-metallurgical processes (leaching followed by extraction using e.g. ion exchange resins, electrochemical and chromatographic methods, dissolution-precipitation methods) and high-temperature approaches (e.g. liquid metal extraction, gas-phase extraction, molten salt methods) (Ang et al., 2017; Hermassi et al., 2021; Kifle & Wibetoe, 2013; Kumari et al., 2021; Li et al., 2022; Makarova et al., 2020; Max-Hansen et al., 2011; Peelman et al., 2016). Most of these methods are expensive, highly technologically advanced, generate dangerous waste and byproducts but yield average/good quality final products or are cheap, simple, generate dangerous waste and byproducts and yield poor quality final products. Currently, there is a renewed interest in the recovery of REE from apatite, particularly from apatite waste generated from the processing of iron ores (Pålsson & Fredriksson, 2012; Sun et al., 2016; Valderrama et al., 2024). New promising methods proposed for chemical extraction of REE in the form of lead phosphates are very effective and do not require physical pre-processing of mineral or waste materials (Sordyl, Staszel, et al., 2023; Sordyl et al., 2024; Staszel et al., 2023; Staszel & Manecki, 2024).

Pyromorphite (Pym, $Pb_5(PO_4)_3Cl$), a chlorine lead-phosphate, belongs to the apatite supergroup of minerals. Naturally occurring Pym is found commonly around polymetallic deposits and as a secondary phase in Pb-contaminated soils. Precipitation of Pym induced by phosphate amendments is also a reclamation method of Pb-polluted soils (Ma et al., 1993; Manecki, 2019; Manecki et al., 2000; Pasero et al., 2010; Tang et al., 2013).

The presence of REE has been broadly investigated in Ca-apatites (Fleet et al., 2000; Fleet & Pan, 1995, 1997a, 1997b; Hughes et al., 1991; Mackie & Young, 1973; Rakovan & Reeder, 1996) mostly due to their applications in petrological studies of mineral deposits (Andersson et al., 2019; Belousova et al., 2002; Bouzari et al., 2016; Harlov, 2015; Zhang et al., 2021). Much less is known about the REE in Pb-apatite. The presence of REE (at ppm levels) has been reported in natural Pym and mimetite ($Pb_5(AsO_4)_3Cl$) specimens (see Markl et al., 2014 and the literature cited therein). Structural position of La in Pym structure has been recently investigated in synthetic analogs (Sordyl, et al., 2023). Still, there is lack of systematic knowledge on the mechanisms of REE-doped Pb-apatite formation. Also, little is known on precipitation of Ce phosphates in the presence of Pb. Coprecipitation of REE with Pym from aqueous solutions is currently of great importance due to potential use in extracting applications (Sordyl et al., 2024). Current state of knowledge regarding REE substitution in Pb-apatite structure is still lacking the specific approach in REE removal effectiveness, if this recovery approach should be used in industrial applications.

It is hypothesized that REE substitution in Pb-apatite should follow approximately the same mechanism as REE substitution in Ca-apatite, due to their similarities in structure (White et al., 2005). Replacement of Ca^{2+} by REE^{3+} requires a coupled substitution. In calcium phosphate apatite representatives, the most common mechanisms for REE substitution are (Pan & Fleet, 2002; Rønsbo, 1989):

$$REE^{3+} + Me^{+} \leftrightarrow 2Ca^{2+} \quad [1]$$

$$REE^{3+} + ZO_4^{4-} \leftrightarrow Ca^{2+} + PO_4^{3-} \quad [2]$$

where in most cases Me^{+} is Na^{+} while ZO_4^{4-} is SiO_4^{4-}. However, Ca and Pb ions differ in ionic radii and their relative positions in apatite crystal structure (Baikie et al., 2014; Kim et al., 2000). This and the

presence of lone electron pair in coordination sphere of Pb^{2+} by phosphate group (Krivovichev, 2003) might result in non-identical substitution mechanisms. Contrarily, structural investigation of La-doped Pym (Sordyl et al., 2023) shows that Pb replacement by La indeed follows assumed substitution mechanism, as in Eq. 1.

The reason for undertaking this research is the appearance of new technology for REE beneficiation by precipitation with pyromorphite. Although this technology has been accepted (MANECKI et al., 2024), little is still known about the phenomena accompanying the precipitation of REE with Pym in various conditions and at different solution concentrations. This research explores for the first time the process and mechanisms of cerium coprecipitation with Pym from aqueous solutions under ambient conditions. Pym was chosen as a representative of Pb-apatite because of its potential application in beneficiation of REE from leachates (Sordyl et al. 2023) and availability of well-tested easy methods of laboratory synthesis (Topolska et al., 2016). Ce was chosen as a representative of Light Rare Earth Elements (LREE) due to its natural abundance in the form of monazite-(Ce) and because this element is often considered a surrogate for actinides behavior in the environment (Darab et al., 2022; Lopez et al., 2003). As a charge-compensating ion, Na^{+} was chosen, assuming coupled heterovalent substitution:

$$Ce^{3+} + Na^{+} \leftrightarrow 2Pb^{2+} \quad [3]$$

due to similar mechanism observed in natural REE-doped Ca-apatite. The effectiveness of Ce removal from solutions by coprecipitation with Pym was explored over a broad range of pH and solution composition while the precipitated solids have also been characterized. Findings from this research will contribute to optimization of modern recovery methods in the field of REE extraction, which might push forward the much-needed evolution of this sector.

2. Materials and methods

2.1. Synthesis

Four sets of batch experiments were conducted that reveal the mechanisms and efficiency of Ce removal by coprecipitation with Pb phosphates: precipitation of Pb phosphates in the presence of Ce

and Cl (Exp. A), precipitation of Pb phosphates in the presence of Cl but in the absence of Ce (Exp. B), precipitation of Ce phosphates in the presence of Cl but in the absence of Pb (Exp. C), and precipitation of Ce and Pb phosphates in the absence of Cl (Exp. D). Each experiment served a different purpose. Experiment A was the main objective – precipitation of Ce-doped pyromorphite (Pym-Ce). Experiment B was designed to observe differences between pure synthetic Pym and Pym-Ce, including the effect of pH. Experiments C and D aimed at investigating the effect of the presence of Pb or Cl, respectively, on precipitation mechanisms of Ce phosphates and effectiveness of Ce removal in relation to results from Exp. A. Composition of solutions used for each experiment is presented in Tab. 1. The concentrations used in the experiments were identical, allowing comparison of product recovery. Relatively high concentrations were used to ensure that the final concentrations were measurable and did not drop to below detection levels (allowing comparison of the effectiveness of removal), and to obtain quantities of solids sufficient for their characterization. Synthesis procedure was identical in all experiments and consisted of simultaneous dropwise introduction of solution 1 (cations) and solution 2 (anions) into the reactor filled with small amount of double-distilled water, using peristaltic pump (1 mL/min flow rate) under constant, vigorous stirring, at ambient temperature in the system open to the atmospheric air (Tab. 1). Solution 1 contained given amount of $Ce(NO_3)_3$ and $Pb(NO_3)_2$ dissolved in 100mL of redistilled water while solution 2 consisted of given amount of NaCl and $NaH_2PO_4 \cdot H_2O$ dissolved in 100mL of redistilled water (Tab. 1). Each experiment was repeated at the pH of 1, 3, 5, 7, 9, and 11 (adjusted with NaOH or HNO_3) to investigate the influence of pH which is often omitted in this kind of experiments. Low concentrated solutions of NaOH and HNO_3 (0.1 - 1.0 M) were used to ensure relative stability of E_H-pH conditions, thus minimizing the possibility of oxidation of Ce(III) to Ce(IV) (Abellan et al., 2017). Redistilled water and the following chemicals were used in the synthesis: $Ce(NO_3)_3 \cdot 6H_2O$ (Acros, purity 99,5%), $Pb(NO_3)_2$ (Chempur, p.a.), NaCl (Chempur, p.a.), $NaH_2PO_4 \cdot H_2O$ (Chempur, p.a.), NaOH (Avantor, p.a.), HNO_3 (Avantor, p.a.).

Tab. 1. Initial concentration of components used for the syntheses.

Exp.	Solution 1		Solution 2		pH range
	[Ce]	[Pb]	[Cl]	[PO_4]	

	mg/L	*mg/L*	*mg/L*	*mg/L*	
A	7600	66700	2800	23200	1 - 11
B	-	66700	2800	23200	1 - 11
C	7600	-	2800	23200	1 - 11
D	7600	66700	-	23200	1 - 11

2.2. Analytical methods

Powder X-ray diffraction (PXRD) patterns were recorded using a Rigaku SmartLab diffractometer in the range of 2–75 °2θ with a step size of 0.05, 1 sec/step, using graphite-monochromatized Cu Kα radiation. Unit cell parameters were calculated using *UnitCell* software (Holland & Redfern, 1997). IR spectra were recorded with Fourier-transform infrared spectroscopy in conjunction with Diffuse Reflectance Infrared Fourier Transform Spectroscopy (DRIFT attachment Praying Mantis, Harrick, USA) using Nicolet 7600 spectrometer in the mid-infrared region (4000 to 400 cm^{-1}). Samples were ground in a mortar with KBr (1 mg of sample with 200 mg KBr) and measured at normal conditions. The spectra were averaged from 64 scans with resolution of 4 cm^{-1}. To investigate the morphology of the obtained materials scanning electron microscopy (SEM) observations were conducted using FEI Quanta 200 FEG SEM equipped with secondary and backscattered electrons detectors, sample prepared on conductive carbon adhesive tape. Chemical analyses were performed by energy dispersive spectrometry (EDS, FEI Quanta) and electron microprobe (EMP) using JEOL JXA-8500F Field emission electron probe microanalyzer (acc. voltage of 15 kV, probe current of 20 nA, a peak count time of 20 s and background count time of 10 s with beam diameter of 1–4 μm), located in the National Electron Microprobe Laboratory at the Department of Earth Sciences at Uppsala University, Uppsala, Sweden. Since the spot size was larger than crystals, the beam was positioned on fine crystal aggregates (fixed in epoxy resin, polished and carbon-coated). Solutions separated after precipitation of phosphates were analyzed by inductively coupled plasma optical emission spectroscopy (ICP-OES).

3. Results and discussion

3.1. Solutions composition

The suspensions were aged after synthesis for 4 weeks before solution sampling to ensure that chemical equilibrium was achieved. Final concentrations of Ce and Pb are presented in Tab. 2.

Precipitation of cerium with phosphates (Exp. A, C and D) has been highly effective in removal of Ce from solution at broad pH range. Concentration of Ce decreased from 3800 mg/L down to 1 mg/L in exp. A (except at pH=1), to below 0.1 mg/L in exp. C, and to 0.02 mg/L in exp. D. The almost complete removal of Ce from solution indicates, among other things, that Ce occurred entirely as Ce^{+3} and possible oxidation to Ce(IV) caused by the open to the air reaction in the presence of HNO_3 does not occur or is negligible. Precipitation of Pym-Ce and Pym resulted also in Pb removal. Final Pb concentrations were lower in the presence of Ce-Pym (Exp. A) than in the presence of pure Pym (control Exp. B). These results may suggest that Ce-doped Pym has lower solubility. This requires confirmation by properly designed solubility experiments. The highest removal efficiency was at alkaline conditions (pH 9 and 11) for both Ce and Pb. Selected solutions (Exp. A at pH = 3 and 11) were sampled every week during aging. No evolution of Pb or Ce concentration was observed (data not shown). This indicates that coprecipitation of Ce with Pym was relatively fast and instantly highly effective in Ce and Pb removal.

Tab. 2. Initial and final concentration illustrating the effectiveness of Ce removal from solutions by precipitation of phosphates in the presence of Pb, Ce and Cl (Exp. A), in the presence of Pb and Cl but in the absence of Ce (Exp. B), in the presence of Ce and Cl but in the absence of Pb (Exp. C), and in the presence of Pb and Ce but in the absence of Cl (Exp. D). Standard deviation in the parenthesis.

	Exp. A		Exp. B		Exp. C		Exp. D	
pH	[Pb]	[Ce]	[Pb]	[Ce]	[Pb]	[Ce]	[Pb]	[Ce]
	mg/L							
1	354 (13)	347 (12)	909 (25)	nd	nd	22.5 (1.0)	5940 (146)	738 (18)
3	15.1 (0.2)	2.05 (0.3)	199 (3.4)	nd	nd	1.25 (0.2)	50.7 (1.3)	1.10 (0.3)
5	3.75 (0.1)	1.23 (0.4)	4.09 (0.5)	nd	nd	<0.1 (-)	169 (3.2)	2.38 (0.4)
7	1.13 (0.1)	1.17 (0.1)	2.48 (0.2)	nd	nd	<0.1 (-)	0.04 (0.01)	0.02 (0.01)
9	<1.0 (-)	1.14 (0.03)	<1.0 (-)	nd	nd	<0.1 (-)	<0.01 (-)	0.02 (0.01)
11	<1.0 (-)	1.0 (0.02)	<1.0 (-)	nd	nd	<0.1 (-)	0.05 (0.01)	0.02 (0.01)
Initial conc.	33400	3800	33400	0	0	3800	33400	3800

nd = not determined.

3.2. Solids characterization

3.2.1. Ce-doped pyromorphite

Synthesis procedure in exp. A and B yielded fine, white or yellowish-white powder that was settling quickly and was easily separated from the remaining solution. Mass of the product of all experiments varied between 8.5 and 9.2 g regardless of the pH. In contrast, the volume of the precipitate settling on the bottom of the reactor (based on visual observations) increased with increasing pH (Fig. S.1 – supplementary materials), potentially indicating decrease in mean particle size. At all pH levels, the precipitate consisted mainly of highly crystalline pyromorphite (Fig. 1). Relatively small admixture of secondary, less crystalline, phase can be observed in exp. A, as evidenced by additional weak reflection near 28.5 °2θ. This peak was attributed to a phase known as mixed lead and REE phosphate ($Ce_2Pb_3(PO_4)_4 \cdot nH_2O$). A detailed description of this phase resulting from synthesis at similar conditions was reported by Staszel et al. (2023). All the peaks correspond to pyromorphite and no additional phases were found. The presence of hydroxylpyromorphite ($Pb_5(PO_4)_3OH$) could not be determined based on X-ray diffraction alone due to similarities in XRD patterns, thus FTIR analysis was performed. No substitution of OH groups for Cl was observed even in the products of syntheses at high pH as evidenced also by lack of hydroxyl bands in FTIR spectra around 3550 cm^{-1} (Fig. S.2). However, the broad hump at 3000-3500 cm^{-1} and a sharper peak at 1640 cm^{-1} are probably due to H_2O present as structural or adsorbed water. Also, absorption bad at ~1385 cm^{-1} could be assigned to CO_3^{2-} stretching indicating partial substitution of carbonates for PO_4^{3-} or/and Cl^- in Pym structure (Kwaśniak-Kominek et al., 2017). These could be partially responsible for low EMP totals which are discussed below.

Diffraction peaks broaden slightly with the increase of pH indicating a decrease in the size of the crystallites and degree of crystallinity. The position of diffraction peaks of Pym-Ce (Exp. A) was systematically shifted compared to control samples towards higher 2θ degrees (Tab. 3). A peak resulting from (300) crystalline plane (at ca. 31° 2θ) was chosen for comparison because the two most intense peaks merged for samples precipitated at high pH. The shift in position of diffraction peaks reflects a slight decrease in the unit cell parameters resulting from the substitution of Ce (Table 4.). Similar was observed for La-doped Pym reported by Sordyl et al. (2023).

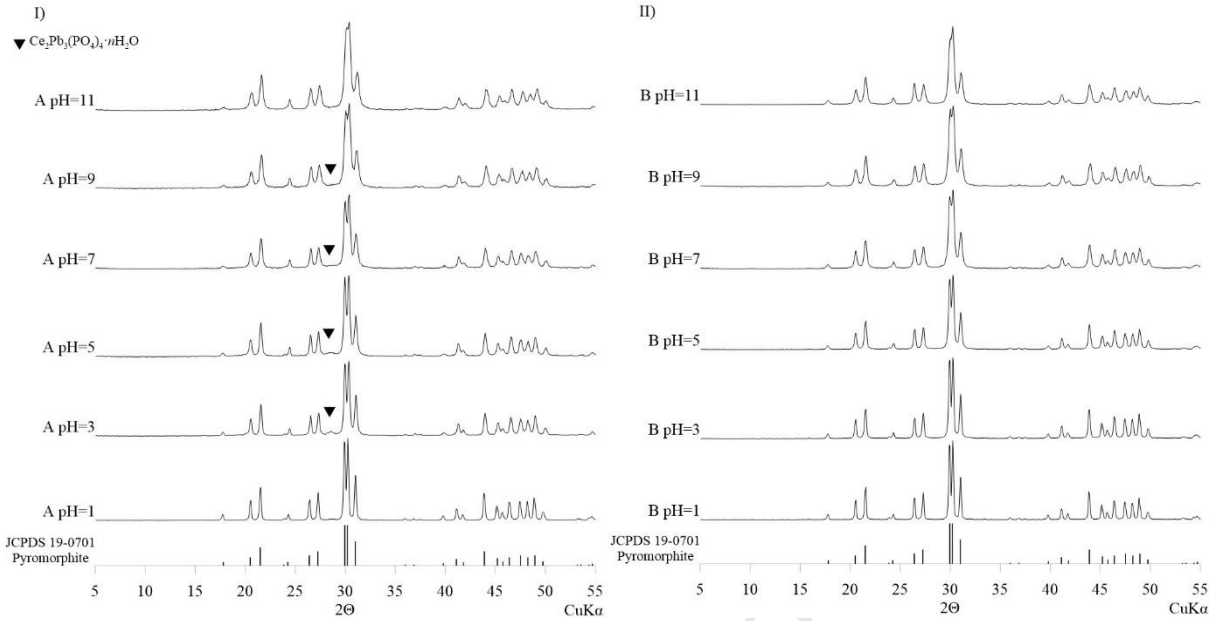

Fig. 1. XRD patterns of Ce-doped Pym (Exp. A, left) and control Pym (Exp. B, right) precipitated at various pH. Weak reflection of additional phase $Ce_2Pb_3(PO_4)_4 \cdot nH_2O$, observed in some patterns resulting from Exp. A around 28.5°2θ is marked with triangles. Peak broadening with increasing pH reflects the decrease in crystal size.

Tab. 3. Shifts in peak (300) position in XRD pattern of Pym-Ce (Exp. A) compared to control Pym (Exp. B) and JCPDS standard.

		Exp. A	Exp. B	Shift between A and B
JCPDS 19-0701		*31.00°2θ*		-
pH	1	30.969	30.973	-0.004
	3	31.012	30.978	+0.034
	5	31.002	30.989	+0.013
	7	31.018	31.003	+0.015
	9	31.092	31.039	+0.053
	11	31.164	31.036	+0.128

Tab. 4. Unit cell parameters of Pym-Ce (Exp. A) compared with control Pym (Exp. B) (hexagonal system).

Phase Exp.	pH	$a = b$ [Å]	c [Å]	V [Å^3]	$a : c$ [-]
A Pym-Ce	1	9.996	7.330	634.259	1 : 0.733
	3	9.982	7.297	629.703	1 : 0.731
	5	9.984	7.296	629.764	1 : 0.731
	7	9.980	7.288	628.624	1 : 0.730
	9	9.954	7.289	625.453	1 : 0.732
	11	9.941	7.275	622.602	1 : 0.732
B control Pym	1	9.991	7.331	633.703	1 : 0.734
	3	9.990	7.326	633.165	1 : 0.733
	5	9.979	7.319	631.213	1 : 0.733
	7	9.976	7.316	630.489	1 : 0.733
	9	9.965	7.310	628.585	1 : 0.735

11	9.989	7.313	631.938	1 : 0.732

SEM imaging confirmed findings from X-ray diffraction analysis. Control Pym exhibited morphology of thick, hexagonal rods, up to 5 μm in length and 3 μm in width (Fig. 2 A). They are terminated with incompletely formed pyramids. A second, smaller, population of Pym crystals was present, being mostly located on the surface of the bigger crystals. As the pH increased, the average crystal size gradually decreased to a point where only sporadic larger Pym crystals, up to 0.5 μm in length, could be distinguished from the microcrystalline mass (Fig. 2 B and C).

Ce-doped Pym exhibited slightly different morphology. The crystals formed elongated needles rather than thick, short and stubby rods. This clearly shows the effect of Ce presence on the morphology of precipitating Pym. At pH = 1, the precipitate contained mainly well-developed, hexagonal needles (Fig. 2 D). Two distinct populations of Pym crystals could be distinguished: long, euhedral crystals up to 10 μm in length and aggregates of smaller needles up to 2 μm in length. Both populations were similar in chemical composition, based on EDS analysis (Tab. S.1). Similar to control Pym, the pH of the synthesis affected the crystals size – smaller crystals were formed at higher pH (Fig. 2 E and F). At pH = 11, individual crystals could hardly be distinguished via SEM imaging.

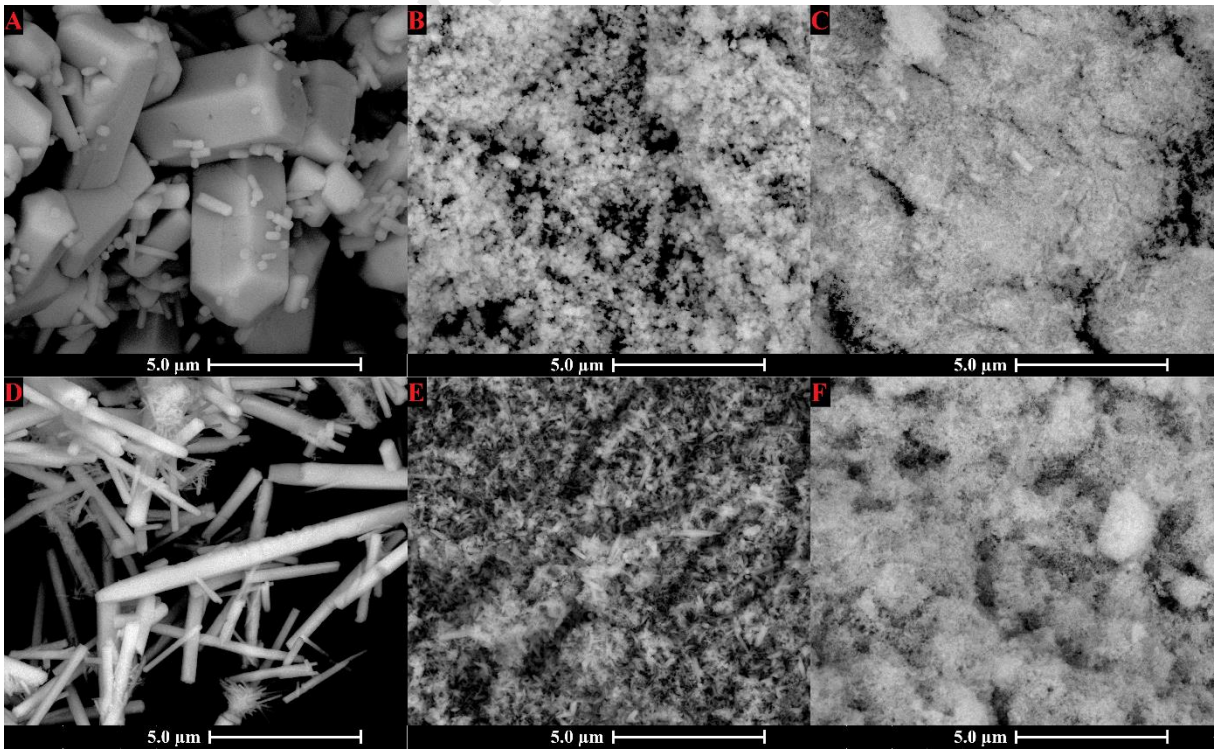

Fig. 2. SEM (BSE) images of control Pym (A-C) and Pym-Ce (D-F) synthesized at pH 1, 5, and 11 (left to right).

Elemental composition of Pym-Ce and control Pym determined by SEM/EDS analysis is presented in Table S.1. Despite relatively poor detection limits and low precision of the EDS spectrometry, the average results and the relative proportion of the elements represent very well pyromorphite composition at all pH. The presence of Na was detected in Pym-Ce and no Na was detected in control Pym confirming the assumed heterovalent substitution mechanism (Eq. 3). For microprobe analyses, Pym-Ce and control Pym synthesized at pH = 3 have been selected as the most representative and composed of relatively large crystals (Tab. S.2). Based on the average results, the chemical formula of Ce-doped Pym was calculated as $Pb_{4.35\pm0.30}Ce_{0.5\pm0.20}Na_{0.15\pm0.04}(PO_4)_{2.93\pm0.05}Cl_{0.89\pm0.13}$. This indicates a slight charge imbalance: excess of positive charge – ca. 0.64+ (assuming all Ce was at 3+ oxidation state, as in the reagent used for the synthesis). Low totals in EMP analysis and inaccuracy in charge balance might result from the imperfection of the microprobe analysis. The other possibility might come from not complete chemical analysis due to possible substitution of PO_4^{3-} or/and Cl^- by CO_3^{2-} (Kwaśniak-Kominek et al., 2017). The analysis was performed on polished aggregate of very fine crystals (smaller than the spot size) immersed in epoxy resin rather than on a polished surface of a single crystal. This made determination of C content impossible. The results, however, are in general agreement with research on La-doped Pym reported by Sordyl et at. (2023), thus proposed general chemical formula of Pym-Ce is $Pb_4(Ce_{0.5}Na_{0.5})(PO_4)_3Cl$.

3.2.2. Rhabdophane-Ce

Precipitates obtained in exp. C (in absence of Pb, all other parameters were the same) were very fine, hard to separate from solution and gel-like in appearance. After drying, solids precipitated at pH 1 and 3 were white, while those obtained at pH = 5 and above were dark grey. The recovery of the dry solid was low and decreased for the precipitates obtained in alkaline solutions, ranging from 0.65 g at pH = 3 to 0.45 g at pH = 11. All the XRD patterns are similar to each other (Fig. 3) and could be assigned to cerium hydrous phosphate $Ce(PO_4)\cdot H_2O$ (Rha-Ce) from rhabdophane group (Mesbah et al., 2014, 2017; Mooney, 1950; Staszel et al., 2023). With increasing pH, the diffraction patterns broadened but individual peaks could still be distinguished. This suggests decrease in mean crystallite size and loss of

crystallinity (Ochiai & Utsunomiya, 2017). Despite the presence of Cl anions during the synthesis, no Cl-containing phase could be assigned to this diffraction pattern. This may suggest that Cl ions do not affect the precipitation of cerium phosphate in the absence of Pb at the assumed conditions of the experiment.

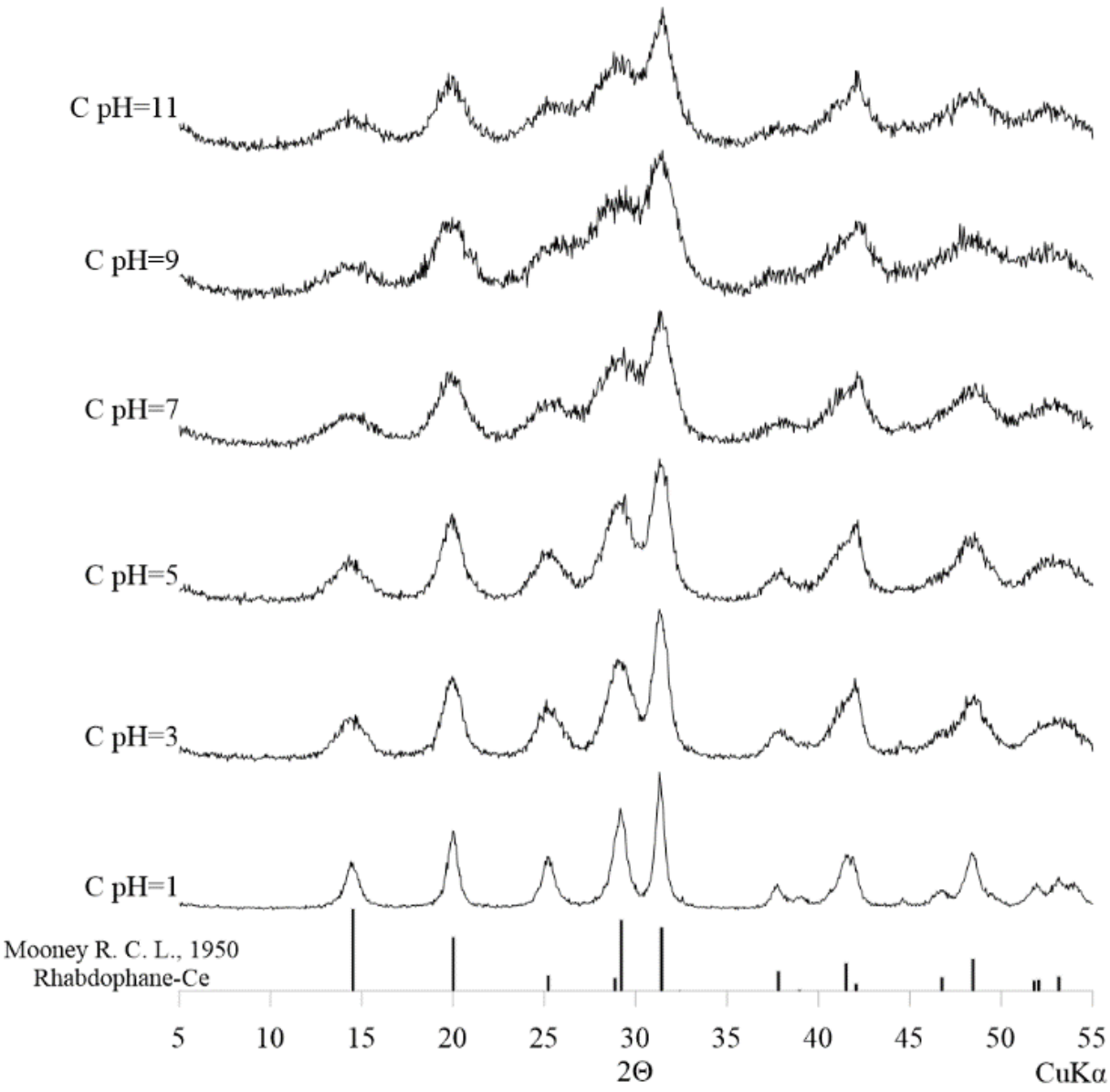

Fig. 3. XRD patterns of phosphates precipitated in the presence of Ce and Cl but in the absence of Pb (Exp. C).

SEM imaging reveals that Rha-Ce precipitated at pH = 1 was relatively well developed in the form of fibrous or needle-like crystals up to 5 μm in length (Fig. 4 A). This is consistent with other

reports on synthetic rhabdophane (Enikeeva et al., 2024; Gausse et al., 2016), slight differences in appearance result from distinct precipitation approaches. As with Pym and in line with the changes in the appearance of the XRD patterns, the size of the crystals decreases with increasing pH (Fig. 4 B).

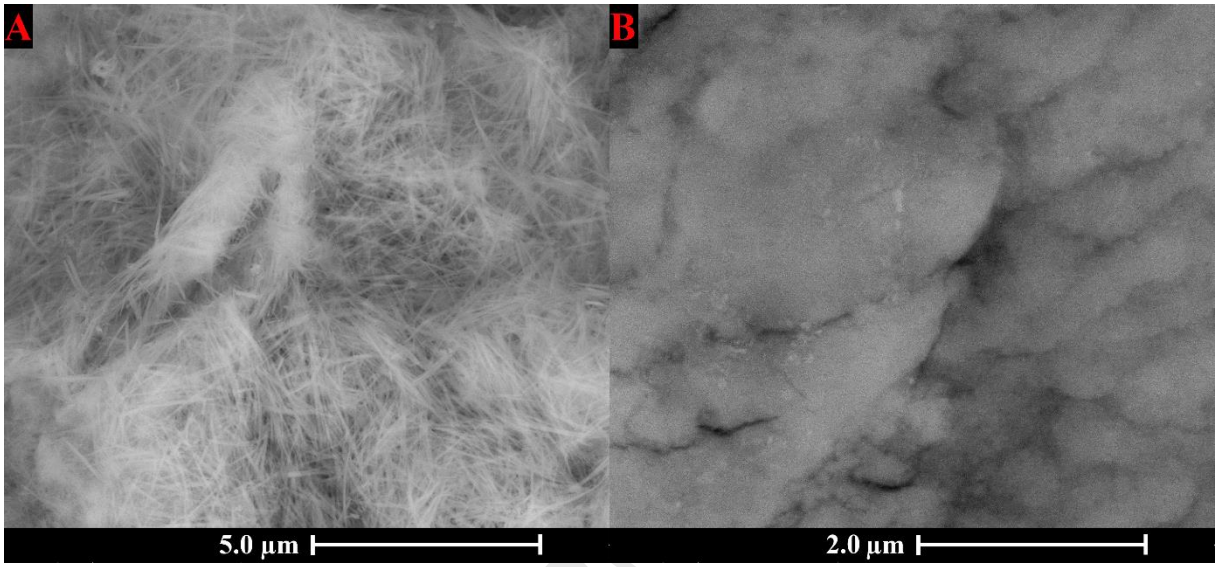

Fig. 4. SEM (BSE) images of rhabdophane-Ce precipitated at pH = 1 (A) and pH = 7 (B).

Chemical composition of precipitates synthesized in the absence of Pb (Exp. C) has been estimated by SEM/EDS analysis (Tab. S.1). No Cl was detected at the detection limit of the method (ca. 0.5 wt. % for Cl), despite its presence in the solution used for the synthesis. The atomic percentages of Ce and P indicated a 1:1 ratio, while the slight excess of O (O : P higher than 4:1 in the PO_4 phosphate group) is probably due to the presence of water molecules in the structure. This is consistent with the composition of rhabdophane $CePO_4 \cdot nH_2O$. The ratio of O to P increased from 4.4 at pH 3 to 5.3 at pH 11 suggesting potentially increasing the degree of hydration. This is in agreement with previous reports on hydrous REE phosphates (Ochiai & Utsunomiya, 2017; Staszel et al., 2023). The exact values of oxygen content should not be taken at face value due to the sample preparation method – carbon adhesive tape should not contain oxygen but could adsorb it during the sample preparation.

3.2.3. Ce and Pb phosphates precipitated in the absence of Cl

Synthesis of Ce and Pb phosphates in the absence of Cl (Exp. D) yielded fine, dense, white (pH = 1 and 3) or yellow (pH ≥ 5) powders that settle quickly and are easily separated from suspension. The recovery varied between 5.7 and 6.7 g, except for solid precipitated at pH = 1 (4.1 g). Diffraction patterns of precipitates obtained at pH = 1 and 3 were distinctly different from the other (Fig. 5). At pH = 1 the only phase detected was 'phosphoschultenite' ('Slt-P') $PbHPO_4$, a phosphate analog of schultenite $PbHAsO_4$. The name of the phase, proposed by Młynarska et al. (2014) and Wudarska et al. (2022) is not yet approved by IMA. No differences or shifts in peak positioning could be observed between this sample and reference card (JCPDS 29-0773). This may indicate a lack of or very small Ce substitution in Slt-P.

The XRD pattern of the solid precipitated at pH=3 does not match any of the known phases containing the elements used in the synthesis. Three high-intensity peaks which dominate XRD pattern, are positioned at 9.71 °2θ (d = 9.11 Å), 19.46 °2θ (d = 4.56 Å) and 29.21 °2θ (d = 3.06 Å). These peak positions and their relative intensities closely resemble the pattern of hopeite (Hop, $ZnZn_2(PO_4)_2{\cdot}4H_2O$). Therefore, the main component of the precipitate was identified as a lead analog of hopeite – $PbPb_2(PO_4)_2{\cdot}nH_2O$. This was associated with small amounts of 'Slt-P' $PbHPO_4$, mixed Pb and Ce phosphate ($Ce_2Pb_3(PO_4)_4{\cdot}nH_2O$), and Hpm $Pb_5(PO_4)_3(OH)$. The solids precipitated at pH range 5 – 11 were composed mostly of Hpm (JCPDS 24-0586). Two additional peaks located near 19.9 and 28.5 °2θ indicate the presence of mixed Pb and Ce phosphate ($Ce_2Pb_3(PO_4)_4{\cdot}nH_2O$), detailed description of which is presented by Staszel et al. (2023). As pH increased, the intensity of these additional peaks decreased, disappearing at pH = 11.

Journal Pre-proof

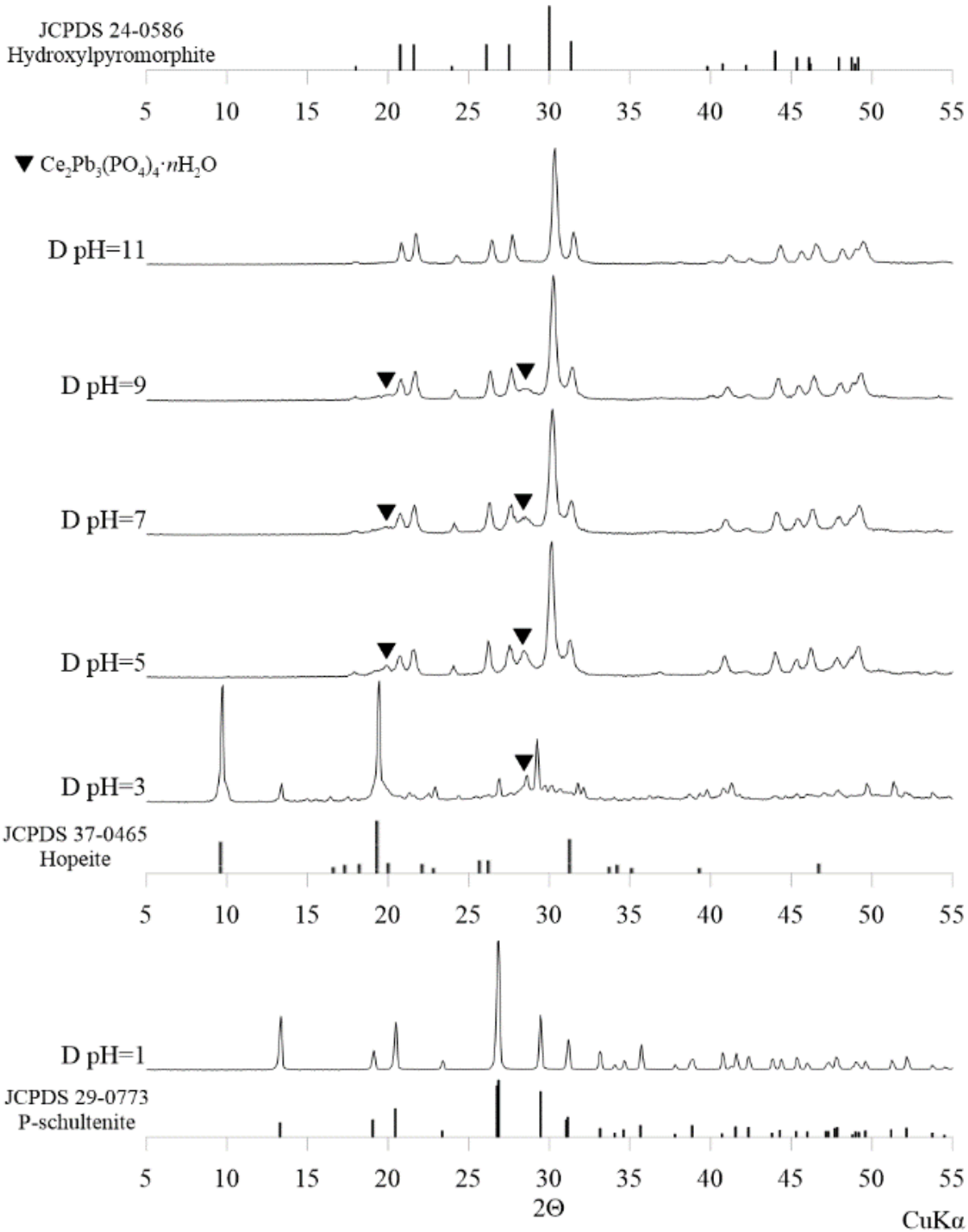

Fig. 5. XRD patterns of Ce and Pb phosphates precipitated in the absence of Cl (Exp. D). Reflections of $Ce_2Pb_3(PO_4)_4 \cdot nH_2O$ are marked with triangles.

SEM image of 'Slt-P' precipitated at pH = 1 in the form of characteristic plates up to 8 μm in size are presented in Fig. 6 A. The morphology is similar to that reported by Wudarska et al. (2022).

Elemental composition estimated with SEM/EDS analysis (Tab. S.1) revealed that it possibly contained small amounts of Ce (ca. 0.5 at%). At pH = 3, two major phases could be distinguished (Fig. 6 B). The large leaf-like euhedral crystals (50 μm in size) were composed of Pb, P, O at molar ratio close to 3:2:8 respectively. This is consistent with the Pb-analog of hopeite ($PbPb_2(PO_4)_2 \cdot nH_2O$) identified with XRD. Smaller crystals were composed of 'Slt-P'. Cerium phosphate, detected in XRD analysis, formed sporadic aggregates of very fine grains below the resolution. In the solids precipitated at pH range of 5 to 11, Hpm was a dominating component (Fig. 6 C and D). The crystal size of hexagonal rods increased with pH reaching up to 2 μm in length at pH = 11. Hpm was sporadically associated with cloudy aggregates composed of phase with ratios of Pb, P and O higher than in $Pb_5(PO_4)_3OH$, suggesting $Ce_2Pb_3(PO_4)_4 \cdot nH_2O$ that was detected in XRD analysis. Therefore, due to the small size of the crystals, it is difficult to determine whether Ce detected at levels as high as 2.5 at% is present in the Hpm structure, or whether this result comes from the surrounding cerium phases.

Journal Pre-proof

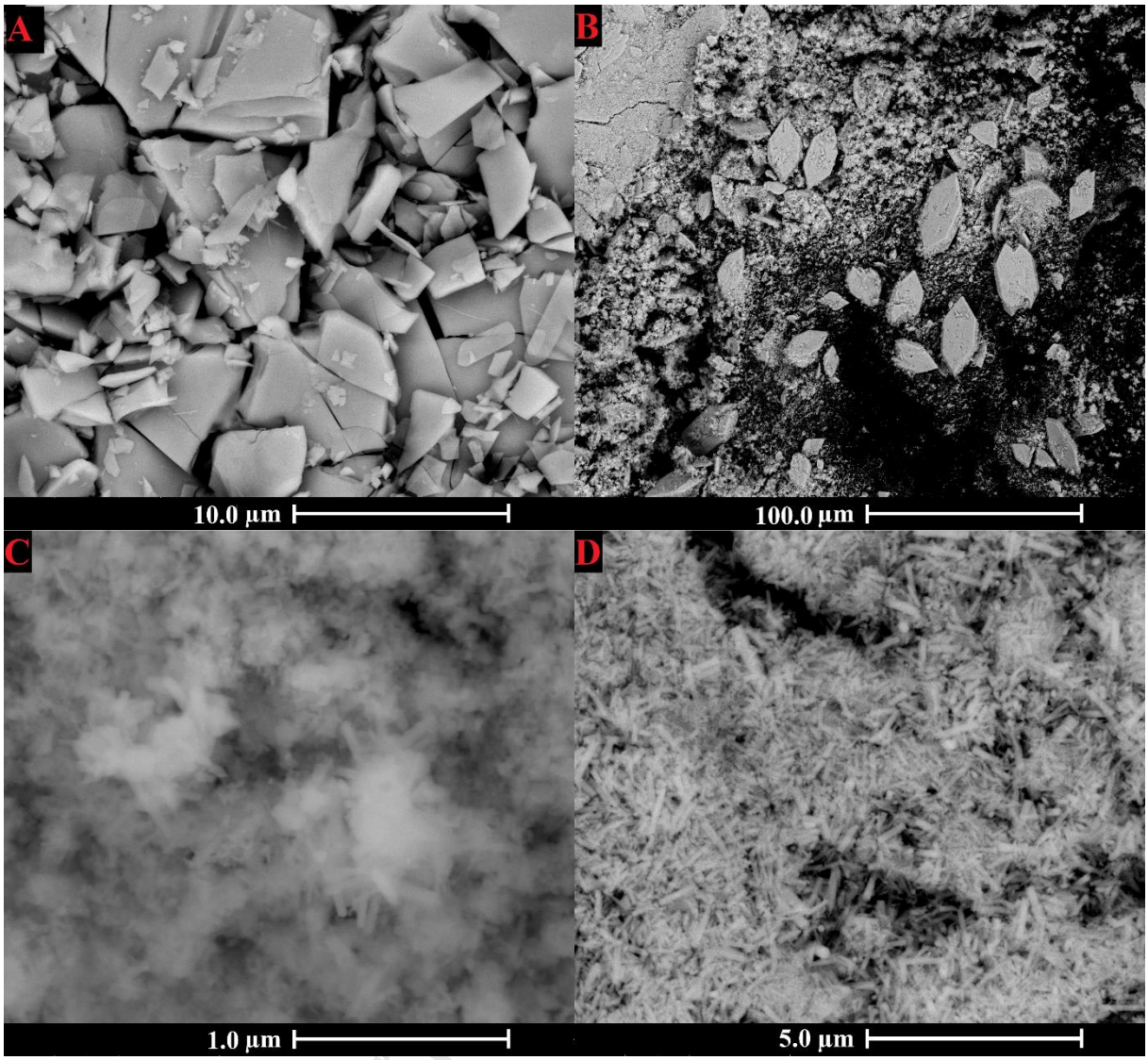

Fig. 6. SEM (BSE) images of (A) 'Slt-P' synthesized at pH = 1, (B) 'Slt-P' and Pb-analogue of hopeite ($PbPb_2(PO_4)_2 \cdot nH_2O$) formed at pH = 3, (C) Hpm precipitated at pH = 5, and (D) Hpm formed at pH = 11.

4. Conclusions

Precipitation of Ce phosphates is of great efficiency in Ce removal from solutions (>99.9%) resulting in formation of fibrous rhabdophane, relatively hard to separate from the suspension. In contrast, precipitation of Ce phosphates in the presence of Pb and Cl results in formation of Ce-doped pyromorphite ($Pb_4(Ce_{0.5}Na_{0.5})(PO_4)_3Cl$) with similar efficiency of Ce removal from solution. This precipitate, over wide pH range, forms high-density, microcrystalline powder containing up to 6 wt% of Ce and is easy to separate from the suspension. The presence of chloride ions is crucial for Pym formation. In absence of Cl, semi-homogenous precipitation occurs only in neutral–alkaline conditions,

resulting in formation of Hpm associated with mixed lead and cerium phosphate. In acidic conditions, synthesis in the absence of Cl has poor efficiency in Ce removal and results in precipitation of various phosphates, from which just one is believed to contain significant amounts of Ce. Therefore, precipitation of Ce-doped pyromorphite is considered most desirable. Further research is needed on the precipitation of REE-doped Pb apatites in the presence of other elements (e.g. Ca, Si, F, As, 2+ and 3+ metals) potentially affecting Ce removal and precipitate properties. Such experiments could strengthen the position of Pb apatites as mediums for REE capture by coprecipitation from aqueous solutions in industrial applications.

5. Declaration of competing interests

The authors declare that they have no known competing financial interests or personal relationships that could have appeared to influence the work reported in this paper.

6. Data availability

Data will be made available on request.

7. Acknowledgments

The authors would like to express their great gratitude to the three anonymous reviewers for their thorough suggestions and comments, which significantly improved the clarity and quality of this manuscript. The authors would like to also acknowledge Katarzyna Wątor and Piotr Rusiniak for the ICP-OES analyses. This research was supported by Polish NCN research grant no. 2021/43/O/ST10/01282.

8. References

Abellan, P., Moser, T. H., Lucas, I. T., Grate, J. W., Evans, J. E., & Browning, N. D. (2017). The formation of cerium(III) hydroxide nanoparticles by a radiation mediated increase in local pH. *RSC Advances*, *7*(7), 3831–3837. https://doi.org/10.1039/C6RA27066B

Andersson, S. S., Wagner, T., Jonsson, E., Fusswinkel, T., & Whitehouse, M. J. (2019). Apatite as a tracer of the source, chemistry and evolution of ore-forming fluids: The case of the Olserum-Djupedal

REE-phosphate mineralisation, SE Sweden. *Geochimica et Cosmochimica Acta*, *255*, 163–187. https://doi.org/10.1016/j.gca.2019.04.014

Ang, K. L., Li, D., & Nikoloski, A. N. (2017). The effectiveness of ion exchange resins in separating uranium and thorium from rare earth elements in acidic aqueous sulfate media. Part 1. Anionic and cationic resins. *Hydrometallurgy*, *174*, 147–155. https://doi.org/10.1016/j.hydromet.2017.10.011

Baikie, T., Schreyer, M., Wei, F., Herrin, J. S., Ferraris, C., Brink, F., Topolska, J., Piltz, R. O., Price, J., & White, T. J. (2014). The influence of stereochemically active lone-pair electrons on crystal symmetry and twist angles in lead apatite-2H type structures. *Mineralogical Magazine*, *78*(2), 325–345. https://doi.org/10.1180/minmag.2014.078.2.07

Belousova, E. A., Griffin, W. L., O'Reilly, S. Y., & Fisher, N. I. (2002). Apatite as an indicator mineral for mineral exploration: Trace-element compositions and their relationship to host rock type. *Journal of Geochemical Exploration*, *76*(1), 45–69. https://doi.org/10.1016/S0375-6742(02)00204-2

Bouzari, F., Hart, C. J. R., Bissig, T., & Barker, S. (2016). Hydrothermal Alteration Revealed by Apatite Luminescence and Chemistry: A Potential Indicator Mineral for Exploring Covered Porphyry Copper Deposits*. *Economic Geology*, *111*(6), 1397–1410. https://doi.org/10.2113/econgeo.111.6.1397

Darab, J. G., Li, H., Bucher, J. J., Icenhower, J. P., Allen, P. G., Shuh, D. K., & Vienna, J. D. (2022). Redox chemistry of plutonium and plutonium surrogates in vitrified nuclear wastes. *Journal of the American Ceramic Society*, *105*(11), 6627–6639. https://doi.org/10.1111/jace.18632

Enikeeva, M. O., Yakovleva, A. A., Proskurina, O. V., Nevedomskiy, V. N., & Gusarov, V. V. (2024). Phase formation under hydrothermal conditions and thermal transformations in the GdPO4-YPO4-H2O system. *Inorganic Chemistry Communications*, *159*, 111777. https://doi.org/10.1016/j.inoche.2023.111777

Fleet, M. E., Liu, X., & Pan, Y. (2000). Rare-earth elements in chlorapatite [Ca10(PO4)6Cl2]: Uptake, site preference, and degradation of monoclinic structure. *American Mineralogist*, *85*(10), 1437–1446. https://doi.org/10.2138/am-2000-1012

Fleet, M. E., & Pan, Y. (1995). Site preference of rare earth elements in fluorapatite. *American Mineralogist*, *80*(3–4), 329–335. https://doi.org/10.2138/am-1995-3-414

Fleet, M. E., & Pan, Y. (1997a). Rare earth elements in apatite: Uptake from H2O-bearing phosphate-fluoride melts and the role of volatile components. *Geochimica et Cosmochimica Acta*, *61*(22), 4745–4760. https://doi.org/10.1016/S0016-7037(97)00292-5

Fleet, M. E., & Pan, Y. (1997b). Site preference of rare earth elements in fluorapatite; binary (LREE+HREE)-substituted crystals. *American Mineralogist*, *82*(9–10), 870–877. https://doi.org/10.2138/am-1997-9-1004

Gausse, C., Szenknect, S., Qin, D. W., Mesbah, A., Clavier, N., Neumeier, S., Bosbach, D., & Dacheux, N. (2016). Determination of the Solubility of Rhabdophanes LnPO4·0.667H2O (Ln = La to Dy). *European Journal of Inorganic Chemistry*, *2016*(28), 4615–4630. https://doi.org/10.1002/ejic.201600517

Harlov, D. E. (2015). Apatite: A Fingerprint for Metasomatic Processes. *Elements*, *11*(3), 171–176. https://doi.org/10.2113/gselements.11.3.171

Hermassi, M., Granados, M., Valderrama, C., Ayora, C., & Cortina, J. L. (2021). Recovery of Rare Earth Elements from acidic mine waters by integration of a selective chelating ion-exchanger and a

solvent impregnated resin. *Journal of Environmental Chemical Engineering*, *9*(5), 105906. https://doi.org/10.1016/j.jece.2021.105906

Holland, T. J. B., & Redfern, S. A. T. (1997). *UNITCELL*: A nonlinear least-squares program for cell-parameter refinement and implementing regression and deletion diagnostics. *Journal of Applied Crystallography*, *30*(1), 84–84. https://doi.org/10.1107/S0021889896011673

Hughes, J. M., Cameron, M., & Mariano, A. N. (1991). *Rare-earth-element ordering and structural variations in natural rare-earth-bearing apatites*. *76*, 1165–1173.

Kifle, D., & Wibetoe, G. (2013). Selective liquid chromatographic separation of yttrium from heavier rare earth elements using acetic acid as a novel eluent. *Journal of Chromatography A*, *1307*, 86–90. https://doi.org/10.1016/j.chroma.2013.07.070

Kim, J. Y., Fenton, R. R., Hunter, B. A., & Kennedy, B. J. (2000). Powder diffraction studies of synthetic calcium and lead apatites. *Australian Journal of Chemistry*, *53*(8), 679–686. https://doi.org/10.1071/ch00060

Krivovichev, S. V. (2003, April 6). *Structural chemistry of basic Pb(II) oxysalt minerals and inorganic compounds*. EGS - AGU - EUG Joint Assembly, Nice, France.

Kumari, A., Dipali, Randhawa, N. S., & Sahu, S. K. (2021). Electrochemical treatment of spent NdFeB magnet in organic acid for recovery of rare earths and other metal values. *Journal of Cleaner Production*, *309*, 127393. https://doi.org/10.1016/j.jclepro.2021.127393

Kwaśniak-Kominek, M., Manecki, M., Matusik, J., & Lempart, M. (2017). Carbonate substitution in lead hydroxyapatite Pb5(PO4)3OH. *Journal of Molecular Structure*, *1147*, 594–602. https://doi.org/10.1016/j.molstruc.2017.06.111

Li, Q., Ji, B., Honaker, R., Noble, A., & Zhang, W. (2022). Partitioning behavior and mechanisms of rare earth elements during precipitation in acid mine drainage. *Colloids and Surfaces A: Physicochemical and Engineering Aspects*, *641*, 128563. https://doi.org/10.1016/j.colsurfa.2022.128563

Lopez, C., Deschanels, X., Bart, J. M., Boubals, J. M., Den Auwer, C., & Simoni, E. (2003). Solubility of actinide surrogates in nuclear glasses. *Journal of Nuclear Materials*, *312*(1), 76–80. https://doi.org/10.1016/S0022-3115(02)01549-0

Ma, Q. Y., Traina, S. J., Logan, T. J., & Ryan, J. A. (1993). In situ lead immobilization by apatite. *Environmental Science & Technology*, *27*(9), 1803–1810. https://doi.org/10.1021/es00046a007

Mackie, P. E., & Young, R. A. (1973). Location of Nd dopant in fluorapatite, Ca5(PO4)3F: Nd. *Journal of Applied Crystallography*, *6*(1), 26–31. https://doi.org/10.1107/S0021889873008009

Makarova, I., Soboleva, E., Osipenko, M., Kurilo, I., Laatikainen, M., & Repo, E. (2020). Electrochemical leaching of rare-earth elements from spent NdFeB magnets. *Hydrometallurgy*, *192*, 105264. https://doi.org/10.1016/j.hydromet.2020.105264

Manecki, M. (2019). Lead in Water and Soil: Speciation, Toxicity, and Treatment Technologies. In P. Maurice (Ed.), *Encyclopedia of Water* (1st ed., pp. 1–13). Wiley. https://doi.org/10.1002/9781119300762.wsts0230

MANECKI, M., MAJKA, J., HÖGDAHL, K., TOPOLSKA, J., SORDYL, J., & ROGALA, P. (2024). *Sposób pozyskiwania metali ziem rzadkich z roztworów pochodzących z ługowania surowców mineralnych i odpadowych* (Patent PL 444079 A1). https://patenty.bg.agh.edu.pl/pelneteksty/PL444079A1.pdf

Manecki, M., Maurice, P. A., & Traina, S. J. (2000). Uptake of aqueous Pb by Cl^-, F^-, and OH^- apatites: Mineralogic evidence for nucleation mechanisms. *American Mineralogist*, *85*(7–8), 932–942. https://doi.org/10.2138/am-2000-0707

Markl, G., Marks, M. A. W., Holzapfel, J., & Wenzel, T. (2014). Major, minor, and trace element composition of pyromorphite-group minerals as recorder of supergene weathering processes from the Schwarzwald mining district, SW Germany. *American Mineralogist*, *99*(5–6), 1133–1146. https://doi.org/10.2138/am.2014.4789

Max-Hansen, M., Ojala, F., Kifle, D., Borg, N., & Nilsson, B. (2011). Optimization of preparative chromatographic separation of multiple rare earth elements. *Journal of Chromatography A*, *1218*(51), 9155–9161. https://doi.org/10.1016/j.chroma.2011.10.062

Mesbah, A., Clavier, N., Elkaim, E., Gausse, C., Kacem, I. B., Szenknect, S., & Dacheux, N. (2014). Monoclinic Form of the Rhabdophane Compounds: $REEPO_4 \cdot 0.667H_2O$. *Crystal Growth & Design*, *14*(10), 5090–5098. https://doi.org/10.1021/cg500707b

Mesbah, A., Clavier, N., Elkaim, E., Szenknect, S., & Dacheux, N. (2017). In pursuit of the rhabdophane crystal structure: From the hydrated monoclinic LnPO 4 .0.667H 2 O to the hexagonal LnPO 4 (Ln = Nd, Sm, Gd, Eu and Dy). *Journal of Solid State Chemistry*, *249*, 221–227. https://doi.org/10.1016/j.jssc.2017.03.004

Młynarska, M., Manecki, M., & Bajda, T. (2014). Structural and Raman spectroscopy studies of schultenite—Phosphoschultenite isomorphic series. *Geology, Geophysics and Environment*, *Vol. 40*(1). http://yadda.icm.edu.pl/baztech/element/bwmeta1.element.baztech-aeb77a41-84f3-473c-aa68-105bf3118a49

Mooney, R. C. L. (1950). X-ray diffraction study of cerous phosphate and related crystals. I. Hexagonal modification. *Acta Crystallographica*, *3*(5), 337–340. https://doi.org/10.1107/S0365110X50000963

Ochiai, A., & Utsunomiya, S. (2017). Crystal Chemistry and Stability of Hydrated Rare-Earth Phosphates Formed at Room Temperature. *Minerals*, *7*(5), 84. https://doi.org/10.3390/min7050084

Pålsson, B. I., & Fredriksson, A. (2012). *Apatite for extraction- II flotation of apatite and rare earth elements from old tailings dumps*. 4064–4074. Scopus.

Pan, Y., & Fleet, M. E. (2002). Compositions of the Apatite-Group Minerals: Substitution Mechanisms and Controlling Factors. *Reviews in Mineralogy and Geochemistry*, *48*(1), 13–49. https://doi.org/10.2138/rmg.2002.48.2

Pasero, M., Kampf, A. R., Ferraris, C., Pekov, I. V., Rakovan, J., & White, T. J. (2010). Nomenclature of the apatite supergroup minerals. *European Journal of Mineralogy*, 163–179. https://doi.org/10.1127/0935-1221/2010/0022-2022

Peelman, S., Sun, Z. H. I., Sietsma, J., & Yang, Y. (2016). Hydrometallurgical Extraction of Rare Earth Elements from Low Grade Mine Tailings. In S. Alam, H. Kim, N. R. Neelameggham, T. Ouchi, & H. Oosterhof (Eds.), *Rare Metal Technology 2016* (pp. 17–29). Springer International Publishing. https://doi.org/10.1007/978-3-319-48135-7_2

Rakovan, J., & Reeder, R. J. (1996). Intracrystalline rare earth element distributions in apatite: Surface structural influences on incorporation during growth. *Geochimica et Cosmochimica Acta*, *60*(22), 4435–4445. https://doi.org/10.1016/S0016-7037(96)00244-X

RØnsbo, Jø. G. (1989). Coupled substitutions involving REEs and Na and Si in apatites in alkaline rocks from the Ilimaussaq Intrusion, South Greenland, and the petrological implications*. *American Mineralogist*, *74*(7–8), 896–901.

Sordyl, J., Chamberlain, C. E., Sweet, T. F. M., Burns, P. C., Cronberger, K., & Manecki, M. (2024). Immobilization of uranium from aqueous solutions by room-temperature precipitation of pyromorphite [Pb5(PO4)3Cl]. *Polyhedron*, 116891. https://doi.org/10.1016/j.poly.2024.116891

Sordyl, J., Rakovan, J., Burns, P. C., Topolska, J., Włodek, A., Szymanowski, J. E. S., Sigmon, G. E., Majka, J., & Manecki, M. (2023). Single-crystal analysis of La-doped pyromorphite [Pb5(PO4)3Cl]. *American Mineralogist*, *108*(12), 2323–2330. https://doi.org/10.2138/am-2022-8664

Sordyl, J., Staszel, K., Leś, M., & Manecki, M. (2023). Removal of REE and Th from solution by co-precipitation with Pb-phosphates. *Applied Geochemistry*, *158*, 105780. https://doi.org/10.1016/j.apgeochem.2023.105780

Staszel, K., Jędras, A., Skalny, M., Dziewiątka, K., Urbański, K., Sordyl, J., Rybka, K., & Manecki, M. (2023). New synthetic [LREE (LREE = La, Ce, Pr, Sm), Pb]-phosphate phases. *Mineralogia*, *54*(1), 58–68. https://doi.org/10.2478/mipo-2023-0006

Staszel, K., & Manecki, M. (2024, April 15). *First evidence of strong REE compatibility with pyromorphite Pb5(PO4)3Cl*. EGU General Assembly 2024, Vienna, Austria. https://doi.org/10.5194/egusphere-egu24-8290

Sun, T., Kennedy, M. W., Tranell, G., & Aune, R. E. (2016). Apatite Concentrate, A Potential New Source of Rare Earth Elements. In N. R. Neelameggham, S. Alam, H. Oosterhof, A. Jha, D. Dreisinger, & S. Wang (Eds.), *Rare Metal Technology 2015* (pp. 145–156). Springer International Publishing. https://doi.org/10.1007/978-3-319-48188-3_17

Tang, P., Zhou, Y., & Xie, Z. (2013). Immobilization of heavy metals in sludge using phosphoric acid and monobasic calcium phosphate. *Journal of Zhejiang University SCIENCE A*, *14*(3), 177–186. https://doi.org/10.1631/jzus.A1200263

Topolska, J., Manecki, M., Bajda, T., Borkiewicz, O., & Budzewski, P. (2016). Solubility of pyromorphite Pb5(PO4)3Cl at 5–65 °C and its experimentally determined thermodynamic parameters. *The Journal of Chemical Thermodynamics*, *98*, 282–287. https://doi.org/10.1016/j.jct.2016.03.031

Valderrama, L., Gómez, O., Pavez, O., & Santander, M. (2024). Recovery of Apatite from Magnetic Concentration Tailings by Flotation. *Minerals*, *14*(5), Article 5. https://doi.org/10.3390/min14050441

White, T., Ferraris, C., Kim, J., & Madhavi, S. (2005). Apatite – An Adaptive Framework Structure. *Reviews in Mineralogy and Geochemistry*, *57*(1), 307–401. https://doi.org/10.2138/rmg.2005.57.10

Wudarska, A., Sordyl, J., Manecki, M., Zawiła, A., & Bajda, T. (2022). Vibrational spectroscopic study of synthetic analogs of schultenite PbHAsO4–"phosphoschultenite" PbHPO4 solid solution series. *Polyhedron*, *211*, 115534. https://doi.org/10.1016/j.poly.2021.115534

Zhang, L., Chen, Z., Wang, F., & Zhou, T. (2021). Apatite geochemistry as an indicator of petrogenesis and uranium fertility of granites: A case study from the Zhuguangshan batholith, South China. *Ore Geology Reviews*, *128*, 103886. https://doi.org/10.1016/j.oregeorev.2020.103886

Journal Pre-proof

Tab. 1. Initial concentration of components used for the syntheses.

Exp.	Solution 1		Solution 2		pH range
	[Ce]	[Pb]	[Cl]	[PO_4]	
	mg/L	*mg/L*	*mg/L*	*mg/L*	
A	7600	66700	2800	23200	1 - 11
B	-	66700	2800	23200	1 - 11
C	7600	-	2800	23200	1 - 11
D	7600	66700	-	23200	1 - 11

Journal Pre-proof

Tab. 2. Initial and final concentration illustrating the effectiveness of Ce removal from solutions by precipitation of phosphates in the presence of Pb, Ce and Cl (Exp. A), in the presence of Pb and Cl but in the absence of Ce (Exp. B), in the presence of Ce and Cl but in the absence of Pb (Exp. C), and in the presence of Pb and Ce but in the absence of Cl (Exp. D). Standard deviation in the parenthesis.

	Exp. A		Exp. B		Exp. C		Exp. D	
pH	[Pb]	[Ce]	[Pb]	[Ce]	[Pb]	[Ce]	[Pb]	[Ce]
	mg/L							
1	354 (13)	347 (12)	909 (25)	nd	nd	22.5 (1.0)	5940 (146)	738 (18)
3	15.1 (0.2)	2.05 (0.3)	199 (3.4)	nd	nd	1.25 (0.2)	50.7 (1.3)	1.10 (0.3)
5	3.75 (0.1)	1.23 (0.4)	4.09 (0.5)	nd	nd	<0.1 (-)	169 (3.2)	2.38 (0.4)
7	1.13 (0.1)	1.17 (0.1)	2.48 (0.2)	nd	nd	<0.1 (-)	0.04 (0.01)	0.02 (0.01)
9	<1.0 (-)	1.14 (0.03)	<1.0 (-)	nd	nd	<0.1 (-)	<0.01 (-)	0.02 (0.01)
11	<1.0 (-)	1.0 (0.02)	<1.0 (-)	nd	nd	<0.1 (-)	0.05 (0.01)	0.02 (0.01)
Initial conc.	33400	3800	33400	0	0	3800	33400	3800

nd = not determined.

Journal Pre-proof

Tab. 3. Shifts in peak (300) position in XRD pattern of Pym-Ce (Exp. A) compared to control Pym (Exp. B) and JCPDS standard.

		Exp. A	Exp. B	Shift between A and B
JCPDS 19-0701		*31.00°2θ*		-
pH	1	30.969	30.973	-0.004
	3	31.012	30.978	+0.034
	5	31.002	30.989	+0.013
	7	31.018	31.003	+0.015
	9	31.092	31.039	+0.053
	11	31.164	31.036	+0.128

Journal Pre-proof

Tab. 4. Unit cell parameters of Pym-Ce (Exp. A) compared with control Pym (Exp. B) (hexagonal system).

Phase		$a = b$	c	V	$a : c$
Exp.	pH	[Å]	[Å]	[Å^3]	[-]
A Pym-Ce	1	9.996	7.330	634.259	1 : 0.733
	3	9.982	7.297	629.703	1 : 0.731
	5	9.984	7.296	629.764	1 : 0.731
	7	9.980	7.288	628.624	1 : 0.730
	9	9.954	7.289	625.453	1 : 0.732
	11	9.941	7.275	622.602	1 : 0.732
B control Pym	1	9.991	7.331	633.703	1 : 0.734
	3	9.990	7.326	633.165	1 : 0.733
	5	9.979	7.319	631.213	1 : 0.733
	7	9.976	7.316	630.489	1 : 0.733
	9	9.965	7.310	628.585	1 : 0.735
	11	9.989	7.313	631.938	1 : 0.732

Journal Pre-proof

- Precipitation of Ce phosphates is of high efficiency in Ce removal from solutions
- Addition of Pb and Cl results in precipitation of crystalline Ce-doped pyromorphite
- Pyromorphite-Ce precipitates over wide pH range (1 – 11)
- 99.99wt% of Pb is transformed into pyromorphite thus the process is not hazardous

Journal Pre-proof